Hindawi
Advances in Condensed Matter Physics
Volume 2017, Article ID 6590424, 6 pages
https://doi.org/10.1155/2017/6590424

Research Article

Tunable Optical Bistability in One-Dimensional Photonic Crystal with a Nonlinear Defect Coupled by Graphene Sheets

Zhiwei Zheng,[1,2] Leyong Jiang,[2] Jun Guo,[1] Xiaoyu Dai,[1] and Yuanjiang Xiang[1]

[1]*SZU-NUS Collaborative Innovation Center for Optoelectronic Science and Technology, Key Laboratory of Optoelectronic Devices and Systems of Ministry of Education and Guangdong Province, College of Optoelectronic Engineering, Shenzhen University, Shenzhen 518060, China*
[2]*College of Physics and Information Science, Hunan Normal University, Changsha 410081, China*

Correspondence should be addressed to Jun Guo; guojun@szu.edu.cn and Xiaoyu Dai; xiaoyudai@126.com

Received 26 June 2017; Accepted 29 August 2017; Published 1 November 2017

Academic Editor: Yan Luo

The optical bistability in one-dimensional photonic crystal (1DPC) with a nonlinear defect is investigated. It is demonstrated that, by introducing graphene layers into the nonlinear defect, the optical bistability in 1DPC can be changed significantly. The hysteresis threshold increases with the number of graphene monolayers and can be lowered or enhanced by tuning the Fermi energy of graphene. On the other hand, the hysteresis width and the nonlinear lateral shift can also be controlled by varying the Femi energy and the number of graphene monolayers. These results may be useful for controlling the optical bistability and nonlinear lateral shift in 1DPCs.

1. Introduction

Optical bistability is a kind of optical phenomenon where one input state can induce two steady transmission states [1]. The input and output intensity in the system can then form a hysteresis loop. One of the simplest examples of bistable systems is a Fabry-Perot cavity filled with a medium which presents saturable absorption or nonlinear dispersion. In recent years, nonlinear photonic crystal formed by introducing Kerr nonlinear material into periodical structure has been proposed to achieve optical bistability [2–5]. Due to the dynamic shifting of the band edge and the strong intensity localized inside the defect mode, the threshold for the onset of optical bistability can be lowered. However, it is hard to control the threshold value in fixed configuration. Hence, the exploration of new optical material with tunable optical properties is important for dynamically tunable optical switches.

Graphene, a single layer of carbon atoms in a hexagonal lattice, has given birth to a new branch of modern optics and new possibilities for manipulating light waves, due to its unique optical and electronic properties [6–9]. Although graphene is atomically thin, it can strongly interact with light over a wide frequency spectrum and has been demonstrated for various photonic applications from photodetectors, ultrafast mode lockers to modulators [10–13]. The linear optical properties in graphene lead to broadband and tunable optical features from IR to visible spectrum [14–16]. The broadband optical property allows graphene to be used as an intrinsically smart optical material for the building block of light controlling system. Recently, the optical bistability of reflection at the interface between graphene and Kerr-type nonlinear substrates was investigated theoretically, and the influence of graphene sheets on the hysteretic response of the nonlinear interface was discussed [17]. It was found that the bistable behavior of the reflected light can be electrically controlled by suitably varying the applied voltage on the graphene. Moreover, the optical bistability in nonlinear photonic crystals exhibits rich nonlinear dynamic behaviors. Hence, the nonlinear photonic crystal coupled with graphene sheets will provide a new scheme to control the hysteresis response of the transmitted light intensity. Moreover, the phase of the transmitted (or reflected) light also exhibits bistable behaviors, thus leading to the hysteresis response of the lateral shift of the transmitted light. We believe that the controllable graphene optical bistable devices could find potential applications in optical all-optical

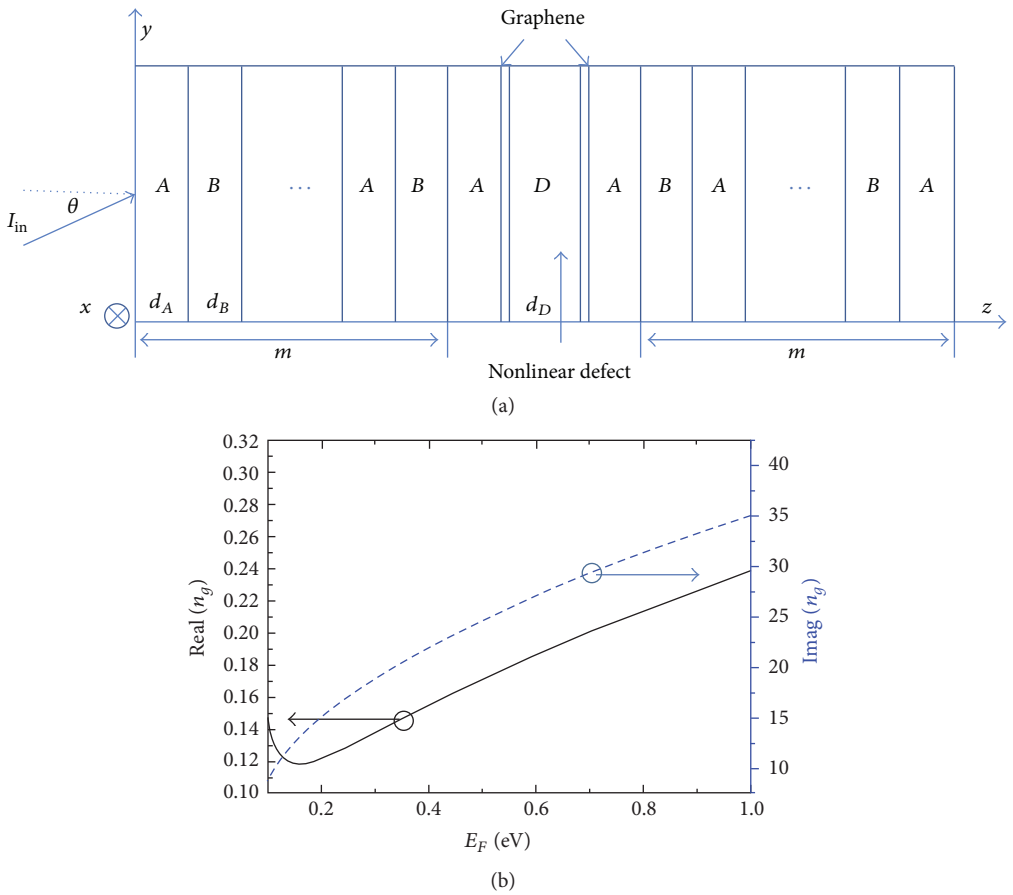

FIGURE 1: (a) The schematic diagram of a 1DPC with a nonlinear defect and graphene layers. m represents the number of periods. (b) Complex effective refractive index of graphene n_g as function of E_F. The solid line and dashed line represent real and imaginary components respectively.

switching [18, 19], optical memory [20], and chemical science [21–23].

2. The Proposed Structure and Simulation Method

This paper is proposed to utilize the tunable features of graphene and to explore the tunable nonlinear transmission features of optical bistability, such as the manipulation of hysteresis threshold, hysteresis width, and nonlinear lateral shift. One-dimensional photonic crystal (1DPC) containing a graphene coupled nonlinear defect is taken as an example.

The structure is shown in Figure 1(a), consisting of two alternate linear layers A and B as 1DPC and a Kerr-type nonlinear layer as defect with effective refraction index $n(I) = n_D + n_2 I$, where n_D is the linear refractive index of the nonlinear defect material, I is the intensity of optical field, and n_2 is the nonlinear refractive. In the following discussion, a normalized unit has been used, which is expressed in units of n_2^{-1}, so that the results will be valid for all Kerr materials with the same n_D and different n_2 [24]. The alternate layers of A, B have high and low linear refractive index n_A, n_B and their thicknesses d_A and d_B satisfy $n_A d_A = n_A d_B = \lambda_{PC}/4$ (the refractive indexes of SiO_2 and TiO_2 are 1.47 and 2.1, resp.). Such a system has a band gap with $2\pi c/\lambda_{PC}$ as the center frequency for the case of normal incidence. The graphene layers are incorporated into both sides of the nonlinear defect layer as shown in Figure 1(a). Both of their graphene thicknesses are set to be $0.34 \times N$ nm, and N indicates the graphene is multilayered with N monolayer(s). The thickness of a monolayer graphene is chosen to be 0.34 nm [25].

Graphene can be characterized by a complex surface conductivity σ, which is a function of angular frequency $\omega = 2\pi c/\lambda$, Fermi energy E_F, carrier scattering rate Γ, and absolute temperature T of the environment. σ is obtained by intraband and interband $\sigma = \sigma_{\text{intra}} + \sigma_{\text{inter}}$ terms, which can be expressed according to the Kubo formula [26]:

$$\sigma_{\text{intra}} = i\frac{e^2 k_B T}{\pi\hbar^2(\omega + i\Gamma)}\left[\frac{E_F}{k_B T} + 2\ln\left(e^{-E_F/k_B T} + 1\right)\right],$$
$$\sigma_{\text{inter}} = i\frac{e^2}{4\pi\hbar}\ln\left[\frac{2E_F - (\omega + i\Gamma)\hbar}{2E_F + (\omega + i\Gamma)\hbar}\right]. \quad (1)$$

In the above formulas, e is the elementary charge, $\hbar = h/2\pi$ is the reduced Planck constant, and k_B is the Boltzmann constant. The Fermi energy of graphene can be manipulated via different approaches, including voltage biasing, exposure to magnetic fields, and chemical doping, which then provide various avenues to control the electronic band property

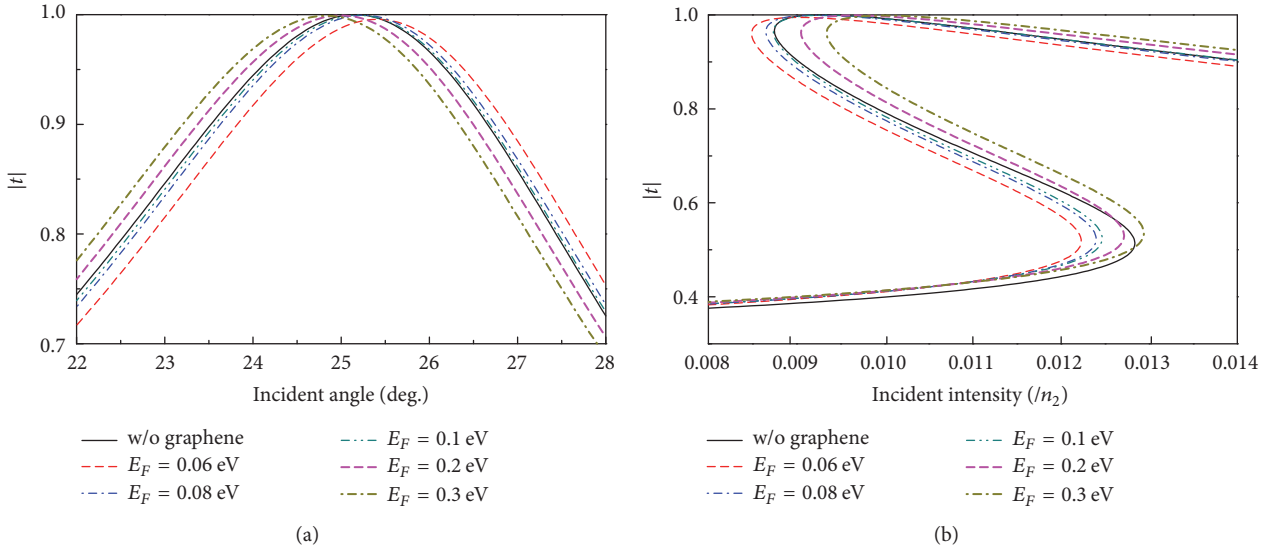

FIGURE 2: (a) $|t|$ versus the angle of incidence for structure without graphene layers (solid curve), with graphene layers of which $E_F = 0.06$ eV (dashed line), $E_F = 0.08$ eV (dash-dotted line), $E_F = 0.1$ eV (dash-dot-dotted line), $E_F = 0.2$ eV (bold dashed line), and $E_F = 0.3$ eV (bold dash-dotted line). (b) $|t|$ versus the incident intensity corresponding to the five situations mentioned in (a).

of graphene [9, 15]. In this research, the graphene carrier scattering rate is assumed to be $\Gamma = 2.4$ THz, the temperature $T = 300$ K, and the incident wavelength $\lambda = 10.6\,\mu$m (the wavelength of CO_2 lasers). In the simulations, graphene is assumed to be a homogenous medium with small thickness, and then the effective refractive index can be derived by $n_g = \sqrt{1 + i\sigma/(\omega\varepsilon_0 d)}$ [15], where $d = 0.34$ nm is the thickness of monolayer graphene. Note that n_g is independent of N, the layer number of a multilayered graphene. Figure 1(b) shows the complex effective refractive index of graphene n_g as function of E_F at the incident wavelength $\lambda = 10.6\,\mu$m. It can be seen that graphene has complex n_g, indicating that the graphene behaves like a very thin metal layer. The solid line implies the real part of n_g, while the dashed line is the imaginary part of n_g. As shown, both of them increase with E_F, and the imaginary part is larger than the real one.

In this paper, we suppose a TE-polarized wave with wavelength λ incident from vacuum upon a finite 1DPC at angle of 27 degrees. In the following discussion, we consider the symmetric multilayer stack consisting of two alternate linear layers A and B as our 1DPC structure. The middle layer is a Kerr-type nonlinear layer. The nonlinear defect layer is sandwiched between two monolayer graphene. The parameters are set as follows: $n_A = 2.1, n_B = 1.47, n_D = 1.594$, $d_D = 3.5\,\mu$m, $\theta = 27^\circ$, $\lambda = 10.6\,\mu$m, and $m = 3$, where d_D and m are the thickness of nonlinear defect layer and the period number of 1DPC, respectively [27]. By applying the transfer matrix method, the characteristic matrix for the nonlinear layer and the composite medium can be calculated. Then the transmission coefficient t can be given by [28]

$$t\left(k_y\right) = \frac{2p_f\left(k_y\right)}{\left[M_{11} + M_{12}p_f\left(k_y\right)\right]p_f\left(k_y\right) + \left[M_{21} + M_{22}p_f\left(k_y\right)\right]}, \quad (2)$$

where $p_f(k_y) = (k^2 - k_y^2)^{1/2}/k$ and $M_{ij}(k_y)$ are the elements of 2×2 matrix $M(k_y)$.

The phase shift of the transmitted beam with respect to the incident beam is defined as [29]

$$\phi\left(k_y\right) = \tan^{-1}\left[\frac{\mathrm{Im}\, t\left(k_y\right)}{\mathrm{Re}\, t\left(k_y\right)}\right], \quad (3)$$

where k_y is the y component of the incident wave vector. Then the lateral shift Δ of the transmitted beam through the multilayered structure is

$$\Delta = \left.\frac{-d\phi\left(k_y\right)}{dk_y}\right|_{\theta=\theta_0}. \quad (4)$$

3. Results and Discussion

First, the angular dependence of transmission coefficient with and without graphene is considered. n_g can be manipulated by setting different E_F values, and $N = 5$ is chosen for the calculation. Figure 2(a) shows the angular dependence of transmission coefficient for structures with and without graphene. As shown, although the graphene layers are very thin, their effects on the nonlinear optical response of the entire structure turn out to be significant. The numerical results for the relation between the normalized incident intensity and transmission coefficient for the same cases in Figure 2(a) are also demonstrated in Figure 2(b), in which a typical S-shaped curve indicates that such a system operates in an optical bistable regime. Figure 2(b) shows that when $E_F = 0.06$ eV, the bistability threshold decreases compared to the case without graphene layers. But when $E_F = 0.3$ eV, the bistability threshold increases. To understand the mechanism that accounts for this variation, the structure

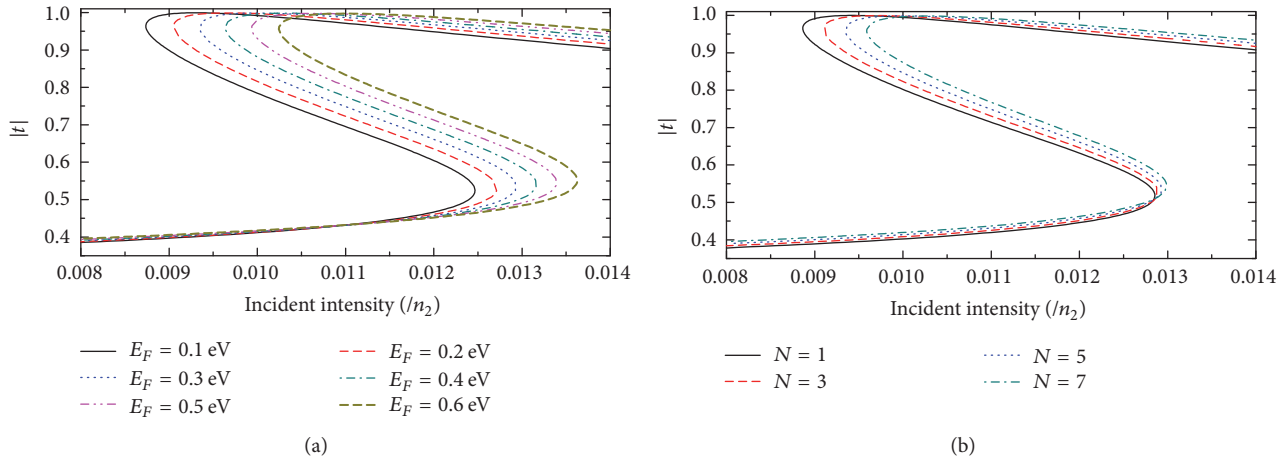

FIGURE 3: $|t|$ versus the incident intensity for graphene with (a) different E_F and $N = 5$ and (b) with different N and $E_F = 0.3$ eV. The incident angle $\theta = 27^\circ$.

in Figure 1(a) can be considered as a resonator filled with nonlinear materials. As shown in Figure 1(b), the effective refractive index of graphene includes the imaginary part and the real part, which indicates that graphene behaves like a thin metal layer. The addition of graphene layers introduces extra positive phase shift and energy loss because of the real part and the imaginary part of n_g. The real part of n_g introduces a positive phase shift, and then the "resonator" length increases. As a result, the intensity dependent nonlinear index change required for switching the system could correspondingly decrease; for example, the intensity required should decrease. The imaginary part of n_g introduces additional energy loss, implying that the input intensity must be higher in order to reach the same "resonator" state. Correspondingly, the intensity required for switching the system should increase. Given that n_g shows both the real part and the imaginary part, each part will impact the nonlinear transmission in an opposite and competitive way, leading to an S shape curve as in Figure 2. As shown in Figure 1(b), both the real part and the imaginary part of n_g increase with E_F, whereas the imaginary part is larger and increases faster than the real part. Therefore, when E_F is smaller, the effect of the real part of n_g is more significant than that of the imaginary part; besides, the intensity required for switching the system decreases compared to the case without graphene. And as E_F becomes larger, the effect of the imaginary part of n_g increases faster than that of the real part. So, with larger E_F, the effect of imaginary part is more significant and the intensity required for switching the system increases. The numerical results shown in Figure 2(b) can prove the above discussion.

Secondly, the effects of graphene layers with different E_F or N on the transmission coefficient are discussed to verify the tunability of graphene layers. Figure 3(a) shows the transmission coefficient dependence on the normalized incident intensity for graphene layers with different E_F. Figure 3(b) is for graphene layers with different N. In Figure 3(a), $N = 5$ while the value of E_F varies. As shown, the hysteresis threshold increases with E_F. It can also be interpreted by the simple resonator analogy mentioned above. When E_F increases, the effect of the imaginary part of n_g (energy loss) becomes more significant, so that both the switch-up and switch-down thresholds will increase. As the switch-up threshold increases faster than the switch-down threshold, the hysteresis width will increase with E_F. In Figure 3(b), the study sets $E_F = 0.3$ eV and varies N and shows the transmission coefficient versus normalized incident intensity. The results are similar to those in Figure 3(a). However, in this case n_g does not change with different N values. The hysteresis threshold increases as N becomes larger. Although n_g is fixed to be constant, the total thickness of multilayered graphene increases with N, so both the additional positive phase shifts and the energy loss increase. Due to the larger imaginary part of n_g, energy loss would increase faster and the hysteresis threshold will increase subsequently. However, the switch-up and switch-down thresholds will increase at the same speed so the hysteresis width will be kept the same.

Lastly, the effects of graphene layers with different E_F or N values on the lateral shift of the transmitted beam are analyzed. Figure 4(a) shows the lateral shift versus the normalized incident intensity for graphene with different E_F, while Figure 4(b) is for the case with different N. It is clear that the hysteretic effect of lateral shift on the incident intensity occurs. As the incident intensity increases, the lateral shift can be switched to a very large value if the incident intensity is larger than the switch-on threshold intensity, which will then enhance the lateral shift. However, as the incident intensity decreases, the lateral shift can be switched to a very small value when the incident intensity is smaller than the switch-down threshold intensity and hence depress the lateral shift. Moreover, the optical properties of graphene sheets exert an important influence on the hysteretic responses of the lateral shifts. Figure 4(a) sets $N = 5$ and varies the value of E_F. As shown, the variation of Δ with different E_F is similar to the transmission coefficient. Both the hysteresis threshold and the hysteresis width increase with E_F. The maximum value of Δ appears near the switch-down threshold and decreases slightly as E_F increases. Figure 4(b) sets $E_F = 0.3$ eV and varies N. As shown, the hysteresis threshold

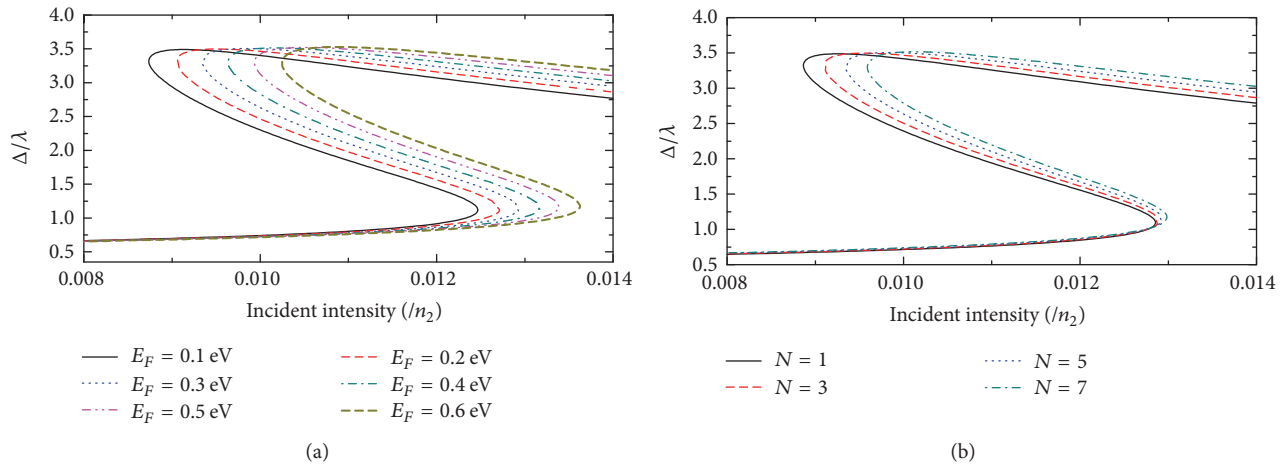

FIGURE 4: The lateral shift versus the normalized incident intensity for graphene with (a) different E_F and $N = 5$ and (b) different N and $E_F = 0.3$ eV. The incident angle $\theta = 27^\circ$.

increases as N becomes larger. Hence, the electrical tunability of optical bistability with graphene could potentially open a new possibility of controlling the lateral shift in a fixed configuration.

4. Conclusions

In summary, this paper mainly explores the effect of multilayered graphene on a nonlinear 1DPC by attaching graphene layers to both sides of the nonlinear defect. It is found that though the graphene layers are very thin, they can significantly modify the nonlinear transmission response, containing the hysteresis threshold, the hysteresis width, and the nonlinear lateral shift. In addition, the influences of graphene layers with different Femi energy and different number of monolayers are analyzed, and the hysteresis threshold shifts by analog of a resonator filled with nonlinear materials are discussed. The results show that the hysteresis threshold increases with Femi energy and the hysteresis width increases at the same time. Besides, the hysteresis threshold also increases with the number of graphene monolayers. These results may be useful for the control of the optical bistability in 1DPCs.

Conflicts of Interest

The authors declare that there are no conflicts of interest regarding the publication of this paper.

Acknowledgments

This work is partially supported by the National Natural Science Foundation of China (Grant nos. 11647135 and 11704119), Hunan Provincial Natural Science Foundation of China (Grant no. 14JJ6007), Scientific Research Fund of Hunan Provincial Education Department (Grant no. 14B119), and the Project Supported for Excellent Talents in Hunan Normal University (Grant no. ET1502).

References

[1] N. M. Litchinitser, I. R. Gabitov, A. I. Maimistov, and V. M. Shalaev, "Effect of an optical negative index thin film on optical bistability," *Optics Letters*, vol. 32, no. 2, pp. 151–153, 2007.

[2] M. Soljacic and J. D. Joannopoulos, "Enhancement of nonlinear effects using photonic crystals," *Nature Materials*, vol. 3, no. 4, pp. 211–219, 2004.

[3] F. Y. Wang, G. X. Li, H. L. Tam, K. W. Cheah, and S. N. Zhu, "Optical bistability and multistability in one-dimensional periodic metal-dielectric photonic crystal," *Applied Physics Letters*, vol. 92, no. 21, Article ID 211109, 2008.

[4] J. Guo, L. Jiang, Y. Jia, X. Dai, Y. Xiang, and D. Fan, "Low threshold optical bistability in one-dimensional gratings based on graphene plasmonics," *Optics Express*, vol. 25, no. 6, pp. 5972–5981, 2017.

[5] S. Chen, L. Miao, X. Chen et al., "Few-Layer Topological Insulator for All-Optical Signal Processing Using the Nonlinear Kerr Effect," *Advanced Optical Materials*, vol. 3, no. 12, pp. 1769–1778, 2015.

[6] A. K. Geim and K. S. Novoselov, "The rise of graphene," *Nature Materials*, vol. 6, no. 3, pp. 183–191, 2007.

[7] Z. Zheng, C. Zhao, S. Lu et al., "Microwave and optical saturable absorption in graphene," *Optics Express*, vol. 20, no. 21, pp. 23201–23214, 2012.

[8] F. Bonaccorso, Z. Sun, T. Hasan, and A. C. Ferrari, "Graphene photonics and optoelectronics," *Nature Photonics*, vol. 4, no. 9, pp. 611–622, 2010.

[9] A. H. Castro Neto, F. Guinea, N. M. R. Peres, K. S. Novoselov, and A. K. Geim, "The electronic properties of graphene," *Reviews of Modern Physics*, vol. 81, no. 1, pp. 109–162, 2009.

[10] M. Liu, X. Yin, E. Ulin-Avila et al., "A graphene-based broadband optical modulator," *Nature*, vol. 474, no. 7349, pp. 64–67, 2011.

[11] H. Zhang, D. Tang, R. J. Knize, L. Zhao, Q. Bao, and K. P. Loh, "Graphene mode locked, wavelength-tunable, dissipative soliton fiber laser," *Applied Physics Letters*, vol. 96, no. 11, Article ID 111112, 2010.

[12] Y. Chen, G. Jiang, S. Chen et al., "Mechanically exfoliated black phosphorus as a new saturable absorber for both Q-switching

and mode-locking laser operation," *Optics Express*, vol. 23, no. 10, pp. 12823–12833, 2015.

[13] G. Gong, H. Zhang, and M. Yao, "Speckle noise reduction algorithm with total variation regularization in optical coherence tomography," *Optics Express*, vol. 23, no. 19, pp. 24699–24712, 2015.

[14] E. Simsek, "Improving tuning range and sensitivity of localized SPR sensors with graphene," *IEEE Photonics Technology Letters*, vol. 25, no. 9, pp. 867–870, 2013.

[15] W. Zhu, I. D. Rukhlenko, L.-M. Si, and M. Premaratne, "Graphene-enabled tunability of optical fishnet metamaterial," *Applied Physics Letters*, vol. 102, no. 12, Article ID 121911, 2013.

[16] S. H. Mousavi, I. Kholmanov, K. B. Alici et al., "Inductive tuning of fano-resonant metasurfaces using plasmonic response of graphene in the mid-infrared," *Nano Letters*, vol. 13, no. 3, pp. 1111–1117, 2013.

[17] Y. Xiang, X. Dai, J. Guo, S. Wen, and D. Tang, "Tunable optical bistability at the graphene-covered nonlinear interface," *Applied Physics Letters*, vol. 104, no. 5, Article ID 051108, 2014.

[18] D. A. Mazurenko, R. Kerst, J. I. Dijkhuis et al., "Ultrafast optical switching in three-dimensional photonic crystals," *Physical Review Letters*, vol. 91, no. 21, p. 213903/4, 2003.

[19] L. Jiang, J. Guo, L. Wu, X. Dai, and Y. Xiang, "Manipulating the optical bistability at terahertz frequency in the Fabry-Perot cavity with graphene," *Optics Express*, vol. 23, no. 24, pp. 31181–31191, 2015.

[20] H. Nihei and A. Okamoto, "Switching time of optical memory devices composed of photonic crystals with an impurity three-level atom," *Japanese Journal of Applied Physics, Part 1: Regular Papers and Short Notes and Review Papers*, vol. 40, no. 12, pp. 6835–6840, 2001.

[21] J. Liu, L. Yu, Z. Zhao et al., "Potassium-modified molybdenum-containing SBA-15 catalysts for highly efficient production of acetaldehyde and ethylene by the selective oxidation of ethane," *Journal of Catalysis*, vol. 285, no. 1, pp. 134–144, 2012.

[22] Y. Luo, V. K. Guda, E. B. Hassan, P. H. Steele, B. Mitchell, and F. Yu, "Hydrodeoxygenation of oxidized distilled bio-oil for the production of gasoline fuel type," *Energy Conversion and Management*, vol. 112, pp. 319–327, 2016.

[23] Q. Xu, H. Xu, J. Chen, Y. Lv, C. Dong, and T. S. Sreeprasad, "Graphene and graphene oxide: Advanced membranes for gas separation and water purification," *Inorganic Chemistry Frontiers*, vol. 2, no. 5, pp. 417–424, 2015.

[24] P. Hou, Y. Chen, X. Chen, J. Shi, and Q. Wang, "Giant bistable shifts for one-dimensional nonlinear photonic crystals," *Physical Review A - Atomic, Molecular, and Optical Physics*, vol. 75, no. 4, Article ID 045802, 2007.

[25] K. S. Novoselov, A. K. Geim, S. V. Morozov et al., "Electric field in atomically thin carbon films," *Science*, vol. 306, no. 5696, pp. 666–669, 2004.

[26] B. Vasic, M. M. Jakovljević, G. Isić, and R. Gajić, "Tunable metamaterials based on split ring resonators and doped graphene," *Applied Physics Letters*, vol. 103, no. 1, p. 011102, 2013.

[27] W. L. Zhang and S. F. Yu, "Bistable switching using an optical Tamm cavity with a Kerr medium," *Optics Communications*, vol. 283, no. 12, pp. 2622–2626, 2010.

[28] J. A. Porto, L. Martín-Moreno, and F. J. García-Vidal, "Optical bistability in subwavelength slit apertures containing nonlinear media," *Physical Review B - Condensed Matter and Materials Physics*, vol. 70, no. 8, pp. 1–81402, 2004.

[29] L. Jiang, Q. Wang, Y. Xiang, X. Dai, and S. Wen, "Electrically tunable Goos-Hänchen shift of light beam reflected from a graphene-on-dielectric surface," *IEEE Photonics Journal*, vol. 5, no. 3, 2013.